GSA Data Repository 2016202

Obliquity-forced climate during the Early Triassic hothouse in China

Mingsong Li, Chunju Huang*, Linda Hinnov*, James Ogg, Zhong-Qiang Chen, and Yang Zhang

*** E-mails: huangcj@cug.edu.cn; lhinnov@gmu.edu.**

This file includes:

1. Supplementary Text

1.1 Gamma-ray as climate proxy

Total gamma-ray intensity (GR) in sedimentary rocks is a proxy for terrestrial weathering. GR of sediments is dominated by potassium (K), uranium (U) and thorium (Th) (e.g., Ruffell and Worden, 2000; Schnyder et al., 2006). K is common in many minerals such as clays, feldspar, mica, and chloride salts. U and Th are concentrated in a number of sedimentary host minerals including clays, feldspar, heavy minerals, and phosphate, and U is often concentrated in organic matter (Schnyder et al., 2006). In the Early Triassic, post-extinction interval sedimentary rocks are depleted of organic matter, and high GR values are attributed to clay-rich sediments, whilst lower GR values are generally linked with coarser-grained rocks and carbonates. Variable clay content may be related to climate change from Milankovitch forcing, e.g., during high eccentricity when hotter summers relative to winters could have resulted in intensified weathering and stronger monsoonal climate. More rainfall and runoff would result in more clay influx into the marine depositional environment, resulting in high GR and U, and vice versa. Modern deep weathering of outcrops can result in leakage of K and U (Osmond and Ivanovich, 1992). Here, new road-cut sections at Daxiakou and Chaohu are fresh which minimizes dissolution from modern weathering (Fig. 1).

1.2 Sea-level fluctuations in the Early Triassic

Recurrent rapid decreases in sea level are known from diverse locations in the Early Triassic, including the South China (Tong and Yin, 1988) and European basins (Gianolla and Jacquin, 1998; Hardenbol et al., 1998), the Canadian Arctic (Embry, 1997) and the Arabian Platform (Haq and Al-Qahtani, 2005). The global sea-level chart indicates several major (>25 m or even >75 m) sea-level falls during the Early Triassic (Hardenbol et al., 1998; Snedden and Liu, 2010), which appear to have been too fast and too widespread to have been caused by tectonics, and were therefore likely triggered by a limno-eustatic process as discussed in the main text.

1.3 La2004 and La2010d astronomical solutions

La2004 (Laskar et al., 2004) and La2010 (Laskar et al., 2011a) are numerical solutions to Earth's astronomical parameters for the past 250 m.y. Solutions La2010a, b and c are based on INPOP08 while

La2010d is based on INPOP06 (Laskar et al., 2011a), which was later shown to be more precise than INPOP08 (Fienga et al., 2011; INPOP=Intégration Numérique Planétaire de l'Observatoire de Paris). La2010d is reliable back to 50-60 Ma (Laskar et al., 2011a). While a strictly accurate astronomical solution is not available for times before 60 Ma (Laskar et al., 2011a; Laskar et al., 2011b; Westerhold et al., 2012), the 1.2 m.y. obliquity modulation persists in both La2004 and La2010d solutions through 249 Ma (Fig. DR5). The obliquity and precession index for the La2010d solution are calculated using the procedure provided in Appendix A of Wu et al. (2013), and setting "datedebut=-249.D0".

1.4 Secular resonance between Earth and Mars orbits and the 1.2 m.y. cycle

Laskar (1990) demonstrated that secular resonance exists between the motions of Earth and Mars corresponding to $(s_4-s_3)-2(g_4-g_3) = 0$, where g_3 and g_4 are secular frequencies contributing to motions of the Earth and Mars orbital perihelia, and s_3 and s_4 are secular frequencies describing motions of their orbital inclinations (3=Earth, 4=Mars). This resonance has been in a librational state, but can evolve into a rotational state, and even to a second librational state, namely $(s_4-s_3)-(g_4-g_3) = 0$. Transitions between these two states are associated with chaotic motions of the planets. The g_4-g_3 term appears in Earth's orbital eccentricity as a ~2.4 m.y. period component, and can be detected in the amplitude modulation envelope of precession-forced stratigraphy; s_4-s_3 appears as a ~1.2 m.y. amplitude modulation in obliquity-forced stratigraphy (Hinnov, 2000). The motions of other, larger planets also have great impact on Earth's paleoclimate change, for example, two of the leading terms in Earth's orbital eccentricity involve Jupiter, g_2-g_5 (405 k.y. period) and g_4-g_5 (95 k.y. period) (Laskar et al., 2004). (Note: 2=Venus, 5=Jupiter). While g_4-g_3 is ranked 8th in amplitude in its direct contribution to Earth's orbital eccentricity, it has a strong effect as a long-period amplitude modulator of the orbital eccentricity arising from simple combinations of Venus terms $[(g_4-g_2)+(g_3-g_2)]$ and Jupiter terms $[(g_4-g_5)+(g_3-g_5)]$ (Matthews et al., 1997). An analogous strong effect occurs from the Earth's orbital inclination terms that modulate the obliquity variation.

2. Methods and Matlab scripts

2.1 GR time-series

GR was measured using a RS-230 BGO Super-SPEC gamma detector. Our measurements used a recording time of 60-120 seconds, and were taken at 5-10 cm intervals at Daxiakou and the majority of Chaohu, and varied from 5 to 20 cm depending on rock exposure in the middle of the Chaohu section. A total of 3007 measurements were taken from the 300 m thick Chaohu section and 1605 measurements from the 135 m thick Daxiakou section.

2.2 Time-series analysis

The GR series were pre-whitened using the Matlab function "smooth.m" with the "lowess" or "rloess" option to remove long-term irregular trends. Evolutionary fast Fourier transform (FFT) spectrograms of the untuned and tuned GR series were calculated using Matlab script "evofft.m" (Kodama and Hinnov, 2014). Based on the indicated wavelengths of the major cycles in the spectral analysis, Gaussian bandpass filtering was applied in AnalySeries 2.0.8 (Paillard et al., 1996) to isolate potential astronomical parameters. The tuned GR series were linearly interpolated to mean time sample rate and resampled in Matlab using script "resample.m". Time series data were analyzed with the multi-taper method (MTM) spectral estimator (Thomson, 1982) using Matlab script "redconf.m" by Dorothée Husson (2014); estimated spectra are compared with red noise models at the 90%, 95% and 99% confidence levels.

2.3 Obliquity power/total power (O/T)

For modeled O/T, we use 10*E+3*O-2*P for both La2004 and La2010d solutions to construct the target model, where E, O and P are standardized (zero mean, unit variance) theoretical orbital eccentricity, obliquity and precession index. The ratio (10:3:2) of E, O and P is based on the relative variance (power) in the eccentricity, obliquity and precession bands of the tuned Chaohu and Daxiakou series (Fig. DR4). Modeled and observed obliquity power was integrated from 1/24 k.y. to 1/45 k.y. frequency band in the estimated power spectra. Total power was integrated from 0 to Nyquist frequency. These power estimates were calculated from 2π MTM power spectra and a 500 k.y. sliding window using Matlab script "pda.m". An extrapolation from 249 to 253 Ma was made for the modeled O/T curves using least-squares fitting (Matlab scripts presented below in Section 2.4, including "deharm.m" in Kodama and Hinnov, 2014).

2.4 Matlab scripts

The Matlab scripts are provided at https://doi.pangaea.de/10.1594/PANGAEA.859147. The zipped file contains the individual Matlab scripts that were used to generate the modeled obliquity amplitude modulations presented in Fig. 3A and Fig. DR5. Each m-file contains header information that explains its functionality in more detail.

3. Figures DR1-DR6

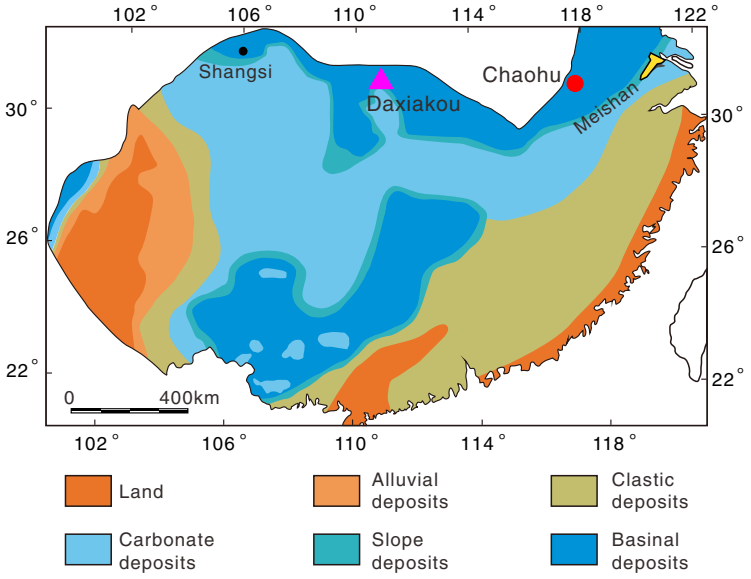

Figure DR1. Early Triassic paleography of South China modified from Feng et al. (1997).

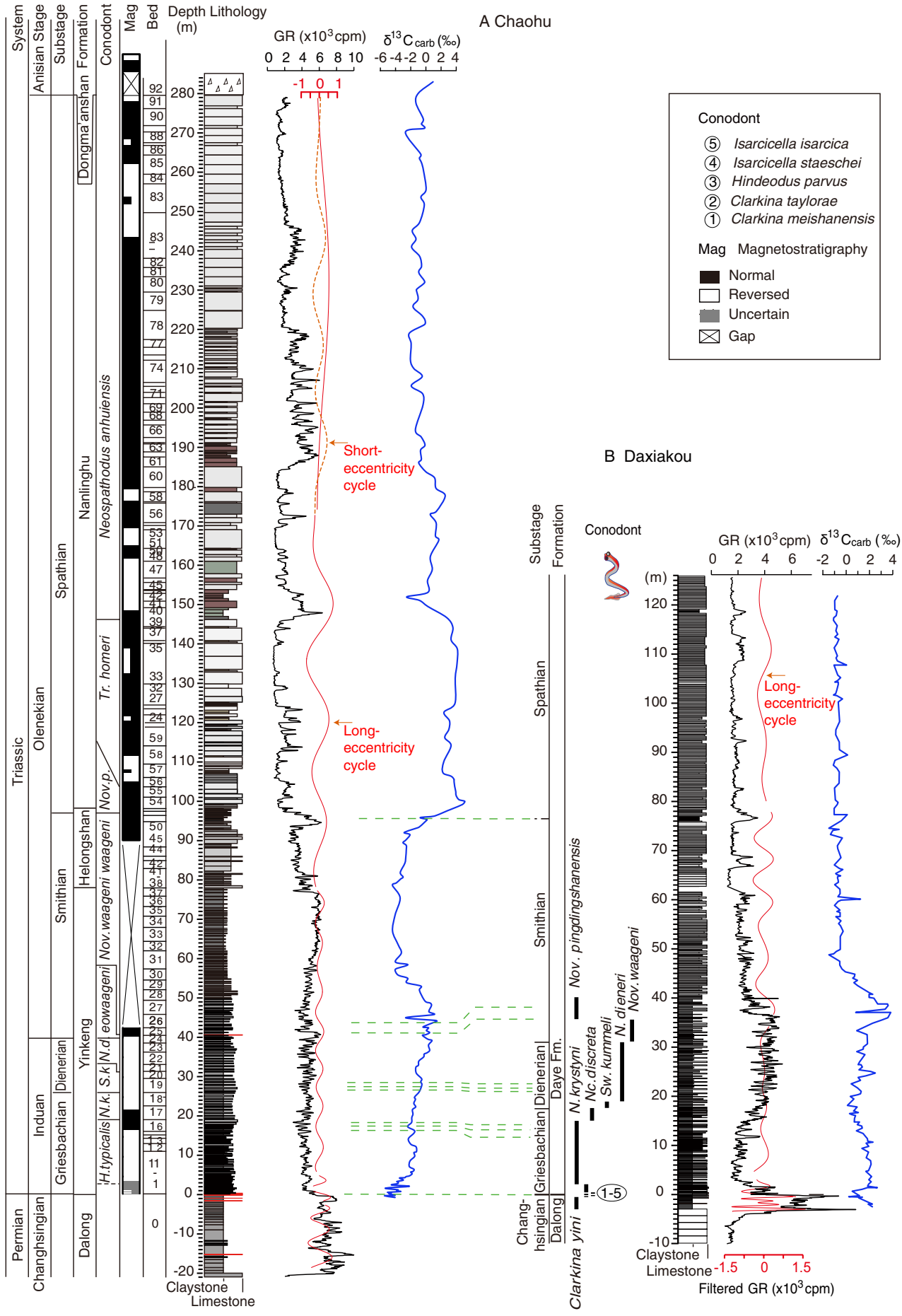
System
Triassic
Permian
Anisian Stage
Olenekian
Changhsingian
Induan
Substage
Spathian
Griesbachian
Dienerian
Smithian
Formation
Nanlinghu
Dongma'anshan
Dalong
Helongshan
Yinkeng
Conodont
Neospathodus anhuiensis
Tr. homeri
Nov.p.
Nov.waageni waageni
Nov.waageni eowaageni
N.d
S.k
N.k.
H.typicalis
Mag
Bed
Depth (m)
Lithology
Claystone
Limestone
A Chaohu
GR (x10³cpm)
δ¹³C carb (‰)
Short-eccentricity cycle
Long-eccentricity cycle
Conodont
① Isarcicella isarcica
② Isarcicella staeschei
③ Hindeodus parvus
④ Clarkina taylorae
⑤ Clarkina meishanensis
Mag Magnetostratigraphy
Normal
Reversed
Uncertain
Gap
B Daxiakou
Substage
Formation
Spathian
Smithian
Dienerian
Griesbachian
Changhsingian
Dalong
Daye Fm.
Nov. pingdingshanensis
N. krystyni
Nc. discreta
Sw. kummeli
N. dieneri
Nov. waageni
Clarkina yini
1-5
(m)
Long-eccentricity cycle
Filtered GR (x10³cpm)

Figure DR2. Correlation of Chaohu and Daxiakou sections with the GR (gamma-ray) logs at each section (Li et al., 2016). Biostratigraphy follows Zhao et al. (2007, 2013). Substages boundaries follow Zhao et al. (2007, 2013) and Li et al. (2016). Paleomagnetic polarity patterns at Chaohu follow Sun et al. (2009) and Li et al. (2016). $\delta^{13}C$ data are from Tong et al. (2007). Filtered GR (red) and interpreted eccentricity cycles are from Li et al. (2016). *H. typicalis*: *Hindeodus typicalis*, *N. k.*: *Neogondolella krystyni*, *Nc. discreta*: *Neoclarkina discreta*; *S. k.*: *Sweetospathodus kummeli*, *N. d.*: *Neospathodus dieneri*, *eowaageni*: *Novispathodus waageni eowaageni*, *Nov. p.*: *Novispathodus pingdingshanensis*, *Tr. homeri*: *Triassospathodus homeri*, Mag: Magnetostratigraphy.

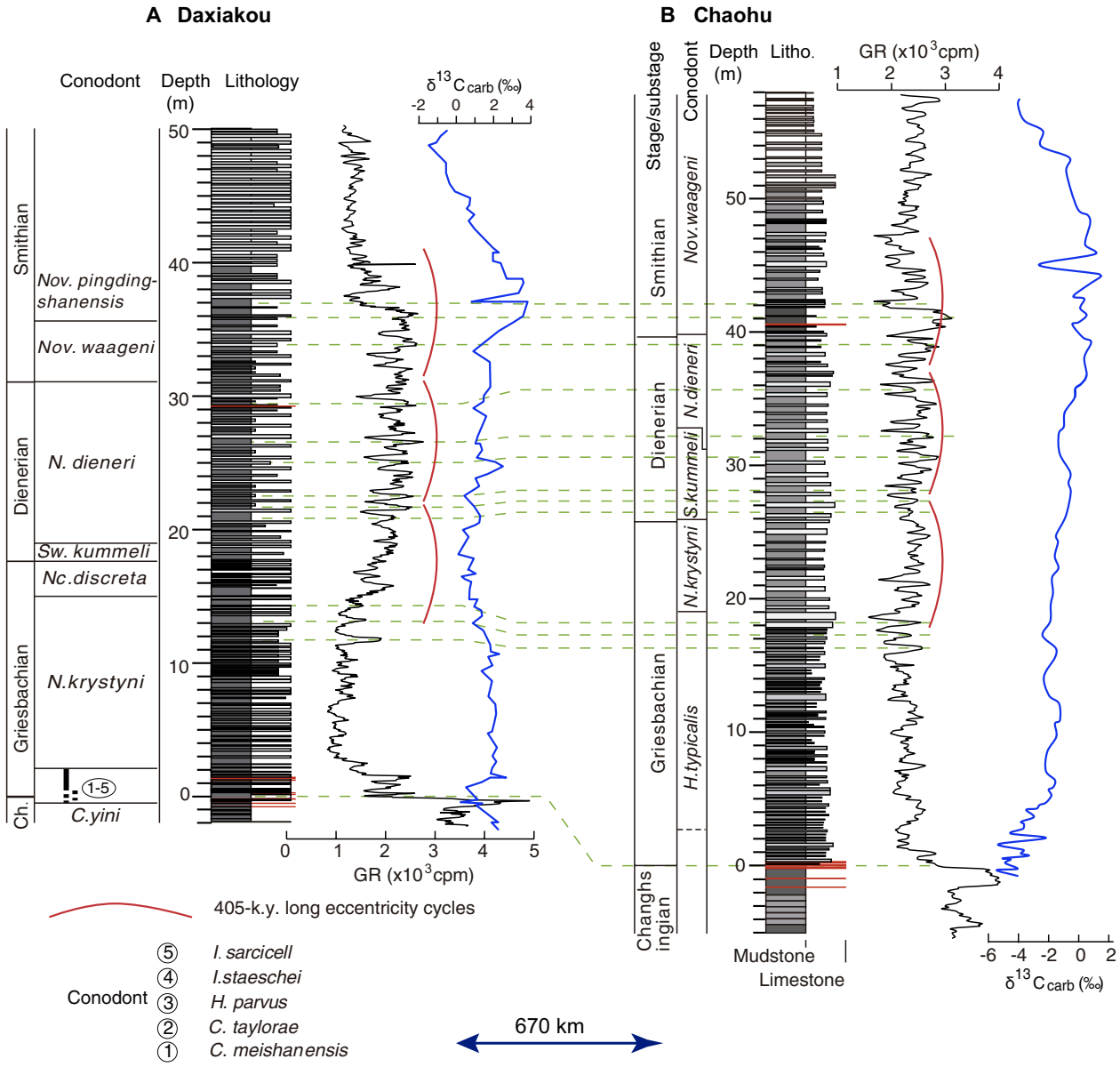

Figure DR3. Correlation of the Daxiakou section and the Chaohu section, South China. The Daxiakou section correlates well with the Chaohu section in gamma-ray (GR), $\delta^{13}C$, lithology and biostratigraphy. Biostratigraphy follows Zhao et al. (2007, 2013). Substages boundaries follow Zhao et al. (2007, 2013). $\delta^{13}C$ data are from Tong et al. (2007). See caption of figure DR2 for abbreviations of conodont zones.

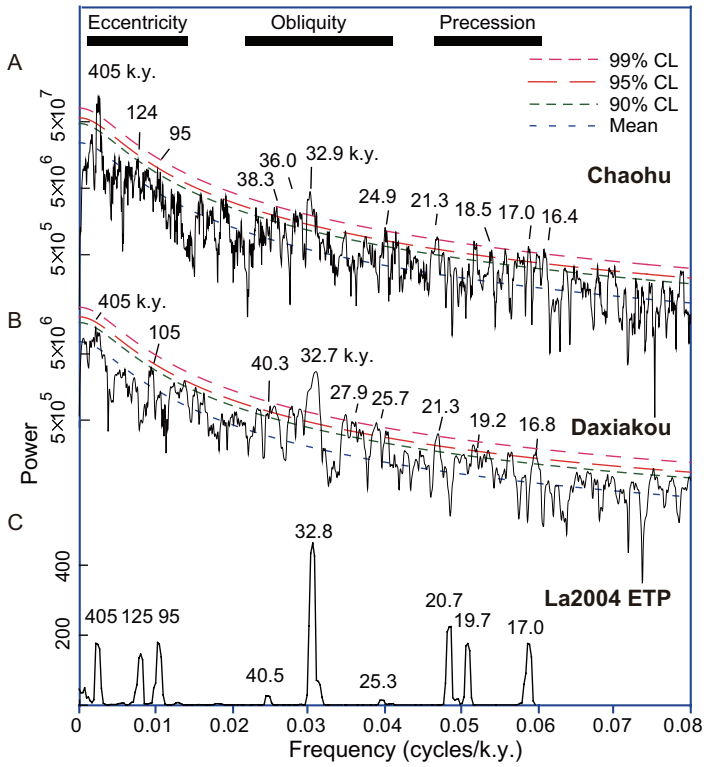

Figure DR4. Spectral analysis. 2π MTM power spectra with red noise models of the 405-k.y. tuned GR time series (Li et al., 2016). A: The complete Chaohu series, less a 15% "lowess" trend, and B: the Triassic portion of the Daxiakou series (0-4.6 m.y.) less a 25% "lowess" trend, both shown with a robust red noise model calculated with linear fitting and a 20% median smoothing window. C: Eccentricity-obliquity-precession time series of the La2004 model (Laskar et al., 2004) from 245 to 249 Ma. CL: confidence level.

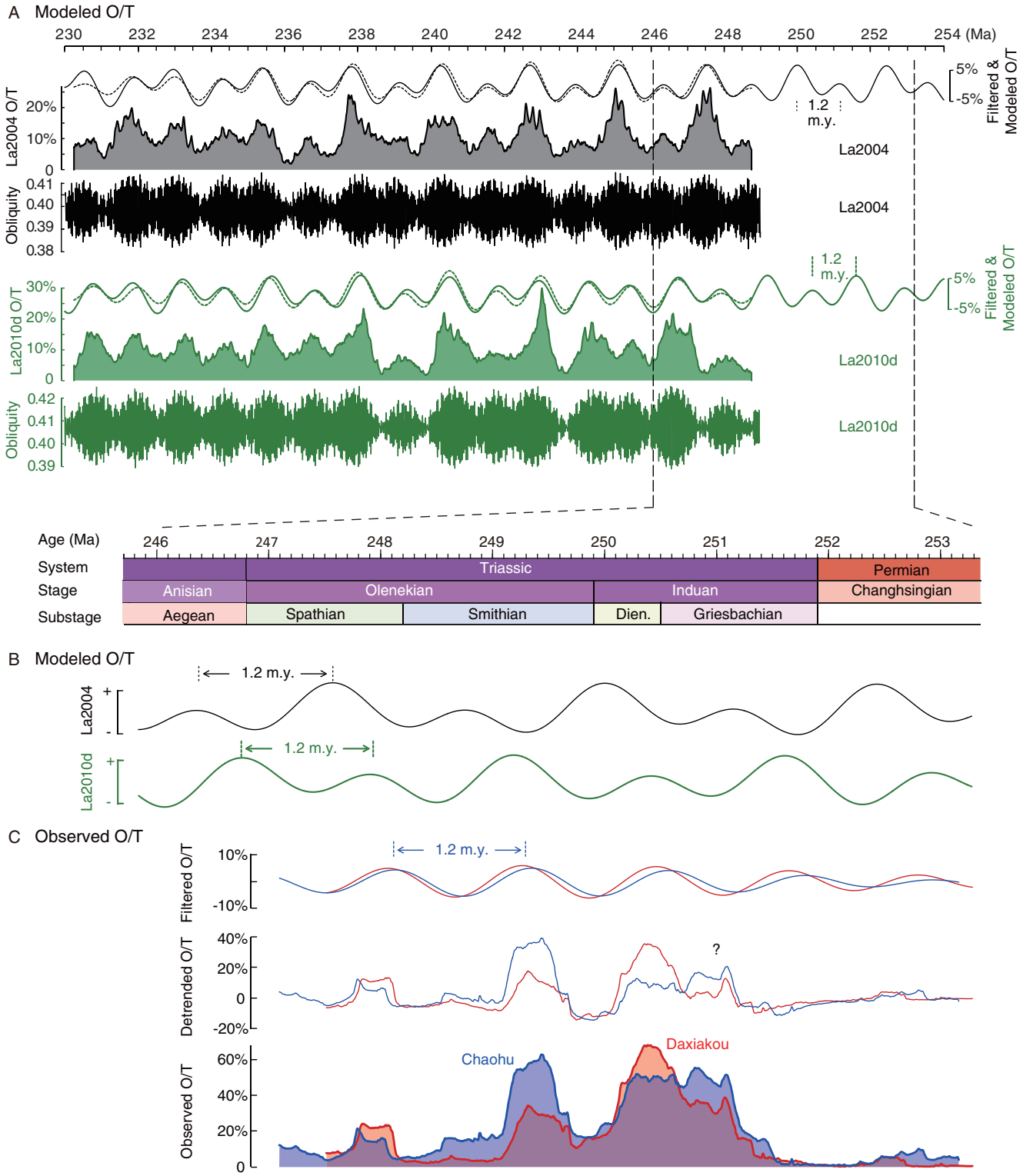

Figure DR5. Modeled and observed obliquity amplitude modulations. A: Obliquity power (1/(24-k.y.) to 1/(45-k.y.) band) compared to total power (0 to Nyquist band), O/T, of the La2004 (black; Laskar et al., 2004) and La2010d (green; Laskar et al., 2011a) ETP series from 230 Ma to 249 Ma (the oldest modeled time provided for the two models) with 2π MTM spectra and a 500 k.y. sliding window (filled area). Also shown are extrapolations to 253 Ma of the modulations (solid lines) computed by least-squares fits to the sum of two Gauss bandpass-filtered outputs of 1.2-m.y. and 2.4-m.y. cycles of O/T from both solutions (dashed lines, passbands: 0.00083±0.0001 and 0.0004±0.00008 cycles/k.y.). B: Extrapolations of the dotted lines from

245.8 to 253.2 Ma as in A. Black: La2004 (Laskar et al., 2004), Green: La2010d (Laskar et al., 2011a), C: From bottom to top: O/T (filled area) of Chaohu (blue) and Daxiakou (red) with a 2.5-m.y.-window "rloess" local regression using Matlab function "smooth.m" (dashed); detrended O/T are O/T less the 2.5-m.y.-window "rloess" trend; and filtered 1.2-m.y. O/T cycles (Gauss filter, passband: 0.00083 ± 0.0001). Dien: Dienerian.

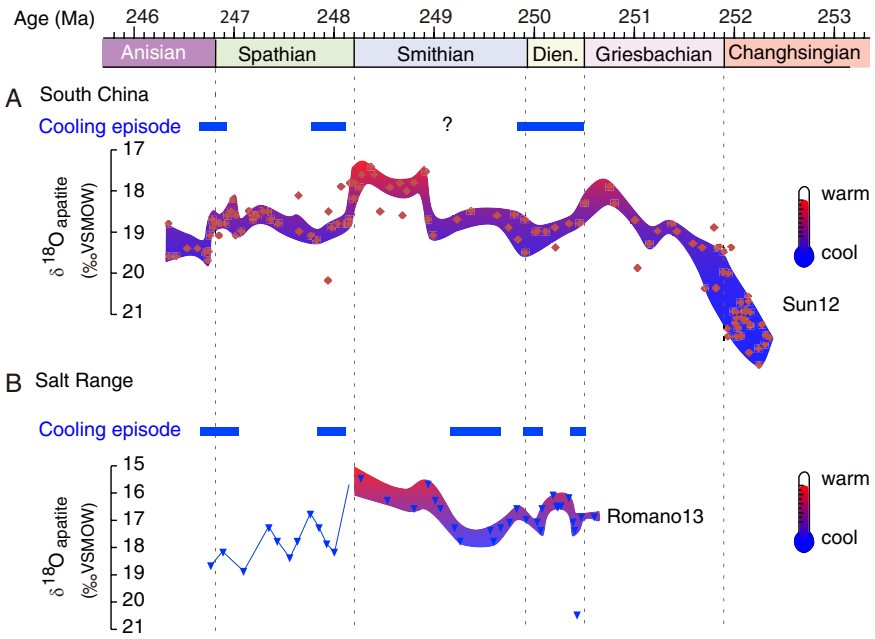

Figure DR6. Cooling episodes in the Early Triassic based on $\delta^{18}O$ of conodont apatite from A: South China (Sun et al., 2012) and B: Salt Range (Romano et al., 2013). Dashed vertical lines indicate substage boundaries used for calibrating $\delta^{18}O$ records to the time scale of Li et al. (2016). Dien: Dienerian.

4. References

Embry, A. F., 1997, Global sequence boundaries of the Triassic and their identification in the Western Canada Sedimentary Basin: Bulletin of Canadian Petroleum Geology, v. 45, no. 4, p. 415-433.

Feng, Z., Bao, Z., and Li, S., 1997, Lithofacies paleogeography of Middle and Lower Triassic of South China, Beijing, Petroleum Industry Press, 222 p.

Fienga, A., Laskar, J., Kuchynka, P., Manche, H., Desvignes, G., Gastineau, M., Cognard, I., and Theureau, G., 2011, The INPOP10a planetary ephemeris and its applications in fundamental physics: Celestial Mechanics & Dynamical Astronomy, v. 111, no. 3, p. 363-385.

Gianolla, P., and Jacquin, T., 1998, Triassic sequence statigraphic framework of western European basins: Special Publication of Society for Sedimentary Geology, p. 643-650.

Haq, B. U., and Al-Qahtani, A. M., 2005, Phanerozoic cycles of sea-level change on the Arabian Platform: GeoArabia, v. 10, no. 2, p. 127-160.

Hardenbol, J., Thierry, J., Farley, M. B., Jacquin, T., Graciansky, P.-C. D., and Vail, P. R., 1998, Mesozoic and Cenozoic sequence chronostratigraphic framework of European basins, In: De Graciansky, P. C., Hardenbol, J., Jacquin, Th., et al., eds., Mesozoic and Cenozoic Sequence Stratigraphy of European Basins, SEPM Special Publication, v. 60, p. 3-13.

Hinnov, L., 2000, New perspectives on orbitally forced stratigraphy: Annual Review of Earth and Planetary

Sciences, v. 28, p. 419-475.

Husson, D., 2014, MathWorks File Exchange: RedNoise_ConfidenceLevels, http://www.mathworks.com/matlabcentral/fileexchange/45539-rednoise-confidencelevels/content/RedNoise_ConfidenceLevels/RedConf.m (April 2014).

Kodama, K. P., and Hinnov, L., 2015, Rock Magnetic Cyclostratigraphy, Wiley-Blackwell, 165 p.

Laskar, J., 1990, The chaotic motion of the solar system: A numerical estimate of the size of the chaotic zones: Icarus, v. 88, no. 2, p. 266-291.

Laskar, J., Fienga, A., Gastineau, M., and Manche, H., 2011a, La2010: a new orbital solution for the long-term motion of the Earth: Astronomy & Astrophysics, v. 532, doi: 10.1051/0004-6361/201116836.

Laskar, J., Gastineau, M., Delisle, J. B., Farrés, A., and Fienga, A., 2011b, Strong chaos induced by close encounters with Ceres and Vesta: Astronomy & Astrophysics, v. 532, doi: 10.1051/0004-6361/201117504.

Laskar, J., Robutel, P., Joutel, F., Gastineau, M., Correia, A. C. M., and Levrard, B., 2004, A long-term numerical solution for the insolation quantities of the Earth: Astronomy & Astrophysics, v. 428, no. 1, p. 261-285.

Li, M., Ogg, J., Zhang, Y., Huang, C., Hinnov, L., Chen, Z.-Q., and Zou, Z., 2016, Astronomical-cycle scaling of the end-Permian extinction and the Early Triassic Epoch of South China and Germany: Earth and Planetary Science Letters. v. 441, p. 10-25.

Matthews, R.K., Frohlich, C., and Duffy, A. 1997, Orbital forcing of global change throughout the Phanerozoic: A possible stratigraphic solution to the eccentricity phase problem, Geology, v. 25, no. 9, pp. 807-810.

Osmond, J., and Ivanovich, M., 1992, Uranium-series mobilization and surface hydrology: Uranium-Series Disequilibrium: Application to Earth, Marine, and Environmental Sciences, Oxford Sciences Publications, Oxford, p. 259-289.

Paillard, D., Labeyrie, L., and Yiou, P., 1996, Macintosh program performs time-series analysis: Eos, Transactions American Geophysical Union, v. 77, no. 39, p. 379-379.

Romano, C., Goudemand, N., Vennemann, T. W., Ware, D., Schneebeli-Hermann, E., Hochuli, P. A., Bruhwiler, T., Brinkmann, W., and Bucher, H., 2013, Climatic and biotic upheavals following the end-Permian mass extinction: Nature Geoscience, v. 6, no. 1, p. 57-60.

Ruffell, A., and Worden, R., 2000, Palaeoclimate analysis using spectral gamma-ray data from the Aptian (Cretaceous) of southern England and southern France: Palaeogeography, Palaeoclimatology, Palaeoecology, v. 155, no. 3–4, p. 265-283.

Schnyder, J., Ruffell, A., Deconinck, J.-F., and Baudin, F., 2006, Conjunctive use of spectral gamma-ray logs and clay mineralogy in defining late Jurassic–early Cretaceous palaeoclimate change (Dorset, U.K.): Palaeogeography, Palaeoclimatology, Palaeoecology, v. 229, no. 4, p. 303-320.

Snedden, J., and Liu, C., 2010, A compilation of Phanerozoic sea-level change, coastal onlaps and recommended sequence designations: Search and Discovery Article #40594. http://www.searchanddiscovery.com/pdfz/documents/2010/40594snedden/ndx_snedden.pdf.html.

Sun, Z., Hounslow, M. W., Pei, J., Zhao, L., Tong, J., and Ogg, J. G., 2009, Magnetostratigraphy of the Lower Triassic beds from Chaohu (China) and its implications for the Induan–Olenekian stage boundary: Earth and Planetary Science Letters, v. 279, no. 3, p. 350-361.

Sun, Y., Joachimski, M. M., Wignall, P. B., Yan, C., Chen, Y., Jiang, H., Wang, L., and Lai, X., 2012, Lethally hot temperatures during the Early Triassic greenhouse: Science, v. 338, no. 6105, p. 366-370.

Thomson, D. J., 1982, Spectrum estimation and harmonic analysis: Proceedings of the IEEE, v. 70, no. 9, p.

1055-1096.

Tong, J., and Yin, H., 1988, The marine Triassic sequence stratigraphy of Lower Yangtze: Science in China Series D: Earth Sciences, v. 41, no. 3, p. 255-261.

Tong, J., Zuo, J., and Chen, Z. Q., 2007, Early Triassic carbon isotope excursions from South China: Proxies for devastation and restoration of marine ecosystems following the end-Permian mass extinction: Geological Journal, v. 42, no. 3-4, p. 371-389.

Westerhold, T., Röhl, U., and Laskar, J., 2012, Time scale controversy: Accurate orbital calibration of the early Paleogene: Geochemistry, Geophysics, Geosystems, v. 13, no. 6, Q06015, doi:10.1029/2012GC004096.

Wu, H., Zhang, S., Jiang, G., Hinnov, L., Yang, T., Li, H., Wan, X., and Wang, C., 2013, Astrochronology of the Early Turonian–Early Campanian terrestrial succession in the Songliao Basin, northeastern China and its implication for long-period behavior of the Solar System: Palaeogeography, Palaeoclimatology, Palaeoecology, v. 385, p. 55-70.

Zhao, L., Chen, Y., and Chen, Z. Q., 2013, Uppermost Permian to lower Triassic conodont zonation from Three George area, South China: Palaios, v. 28, no. 8, p. 509-522.

Zhao, L., J, O. M., Tong, J., Sun, Z., Zuo, J., Zhang, S., and Yun, A., 2007, Lower Triassic conodont sequence in Chaohu, Anhui Province, China and its global correlation: Palaeogeography, Palaeoclimatology, Palaeoecology, v. 252, no. 1, p. 24-38.